Prediction of a Highly Activated State of CO Adsorbed on an Al/Fe(100) Bimetallic Surface[†]

D. E. Jiang[‡,§] and Emily A. Carter*[,||]

Department of Chemistry & Biochemistry, Box 951569, University of California, Los Angeles, California 90095-1569, and Department of Mechanical and Aerospace Engineering and Program in Applied and Computational Mathematics, Princeton University, Princeton, New Jersey 08544-5263

Received: October 25, 2005

Using periodic slab density functional theory, we investigate CO adsorption, diffusion, and dissociation energetics on a monolayer of Al covering Fe(100) [Al/Fe(100)]. We predict a weakly chemisorbed state of CO to exist on Al/Fe(100), with CO adsorbing on the 4-fold hollow site in a very tilted fashion. This state is predicted to have an extremely low CO stretching frequency of only 883 cm^{-1}, indicating a dramatically weakened CO bond relative to gaseous CO, even though the molecule is predicted to bind to Al/Fe(100) quite weakly. We predict that dissociation of CO starting from this weakly adsorbed state has a barrier of only ∼0.35 eV, which is ∼0.70 eV lower than that on Fe(100). To understand how the underlying substrate changes the electronic properties of the supported Al monolayer, we compare CO adsorption on Al/Fe(100) to its adsorption on analogous pure Al(100) surfaces. This highly activated yet weakly bound state of CO on Al/Fe(100) suggests that Al/Fe(100) could be an effective low-temperature bimetallic catalyst in reducing environments.

1. Introduction

Bimetallic surfaces offer unique geometries and electronic properties for surface chemistry and catalysis.[1−3] Different types of bimetallic systems have been explored experimentally in the past 20 years. Here we focus on a special kind of bimetallic surface: a supported metal monolayer on another metal substrate. Such a monolayer exhibits electronic properties distinct from its bulk counterpart, resulting from two effects: the strain in the monolayer caused by the substrate and the mixing of its metallic states with the substrate. The altered electronic structure can in turn produce unusual surface chemistry. For example, Campbell and Goodman[4] showed that an overlayer of Al on Ru(0001) [Al/Ru(0001)] greatly changed CO thermal desorption spectra relative to clean Ru, and later, using angle-resolved photoelectron spectroscopy, Pelzer et al.[5] showed that CO adsorbs in a tilted state on Al/Ru(0001) instead of upright as on Ru(0001). Yates and co-workers[6] found, with high-resolution electron energy loss spectroscopy (HREELS), an adsorption state of CO with a quite low vibrational frequency of 1370−1430 cm^{-1} on Ni/Al(111), not observed on Ni(111) or Al(111). They proposed that it might be a Ni−C−O−Al species. Koel and co-workers[7,8] found that the heat of adsorption of CO decreases dramatically from 1.47 eV on Pd(111) or 1.58 eV on Pd(100) to 0.62 eV on Pd/Ta(110) and to 0.87 eV on Pd/Mo(100). As an example of altered chemistry, Chen and co-workers[9,10] observed that cyclohexene is weakly π bonded on Ni/Pt(111), but di-σ-bonded on pure Pt(111) or Ni(111), leading to a different hydrogenation pathway for cyclohexene on Ni/

Pt(111). They later used density functional theory (DFT) to understand how the metal-supported monolayer affects the surface chemistry.[11,12]

Activation of the CO bond is an important step in various industrial processes such as Fischer−Tropsch catalysis.[13] Many transition metals can break the CO bond, despite its large bond strength of 11.2 eV.[14] The Blyholder model[15] of CO σ donation and metal π back-bonding has often been employed to explain the initial adsorption interaction between CO and transition metals.[16] The red shift of the CO stretching frequency relative to its gaseous value (2170 cm^{-1}) has been used as an indicator of the extent to which the CO bond is weakened on metal surfaces. Transition metals with only partially filled d states, such as Fe and Cr[17,18] are very effective at dissociating CO and also exhibit very low C−O stretching frequencies.

Another means of weakening the CO bond is to dope the metal surface with alkali metals. For example, when potassium is coadsorbed with CO on Al(100), a very low CO stretching frequency (1060 cm^{-1}) is observed.[19,20] This frequency is even lower than the 1210 cm^{-1} measured for the tilted state of CO on Fe(100).[21] CO dissociation on K/Al(100) occurs upon heating to 190 K, where the CO adsorption state associated with the low frequency is thought to be the precursor leading to dissociation. This correlation of a low-frequency CO adsorption state with facile dissociation is similar to Fe(100), where CO is chemisorbed and dissociates around room temperature (RT). By contrast, CO is only physisorbed on clean Al(100) at low temperatures and desorbs without dissociating at RT.[22] The stark contrast in CO chemisorption behavior between pure Fe and pure Al, as well as the changes in behavior observed for supported metal monolayers, motivates the present investigation of how a monolayer of Al on Fe(100) affects CO adsorption and dissociation.

In this work, we use periodic DFT to characterize adsorption sites, diffusion barriers, and dissociation pathways for CO on a

* Corresponding author. Phone: (609) 258-5391. Fax: (609) 258-5877. E-mail: eac@princeton.edu.
† Part of the special issue "Charles M. Knobler Festschrift".
‡ University of California, Los Angeles.
§ Present address: Oak Ridge National Laboratory, P.O. Box 2008 MS6367, Oak Ridge, TN 37831-6367.
|| Princeton University.

monolayer of Al on Fe(100). We also compare the chemistry of CO on Al/Fe(100) with pure Al(100). The paper is organized as follows. In section 2, we outline the theoretical method employed. Results and discussion for CO adsorption, diffusion, and dissociation are presented in section 3. We summarize and conclude in section 4.

2. Calculational Methods

We perform first-principles calculations based on density functional theory (DFT).[23,24] The Vienna ab Initio Simulation Package (VASP) is used to solve the Kohn–Sham equations with periodic boundary conditions and a plane-wave basis set.[25,26] Here we employ Blöchl's all-electron projector augmented wave (PAW) method,[27] as implemented by Kresse and Joubert,[28] within the frozen core approximation. For the treatment of electron exchange and correlation, we use the PBE[29] and RPBE[30] forms of the generalized gradient approximation (GGA). RPBE slightly modifies PBE and has been shown to produce better adsorption energetics.[30] Since PBE is known to be reliable for geometry optimization,[29] we optimize all the structures with PBE and perform static calculations with RPBE for the PBE-optimized structures.

We use a kinetic energy cutoff of 400 eV for the plane-wave basis in all calculations, which converges the total energy to $\sim$1 meV/atom for the primitive cell of bulk Fe. The Monkhorst–Pack scheme is used for the k-point sampling,[31] with a converged k-mesh of $15 \times 15 \times 15$ for the primitive cell of bulk Fe. The first-order Methfessel–Paxton method[32] is used for the Fermi-surface smearing, with a width of 0.1 eV in order to obtain accurate forces. With these parameters, we obtain an equilibrium lattice constant ($a_0 = 2.834$ Å), bulk modulus ($B = 174$ GPa), and local magnetic moment ($M = 2.20$ μ_B) for ferromagnetic body-centered-cubic (bcc) Fe. The results agree very well with previous PAW–GGA calculations and experiment ($a_0 = 2.86$ Å, $B = 168$ GPa, $M = 2.22$ μ_B).[33] Placing a CO molecule in a 10 Å cubic box and using the PBE functional, we obtain an equilibrium bond length ($R_e = 1.14$ Å), bond dissociation energy ($D_e = 11.5$ eV), and harmonic vibrational frequency ($\nu_e = 2158$ cm^{-1}) for CO that agrees fairly well with experiment ($R_e = 1.13$ Å, $D_e = 11.2$ eV, $\nu_e = 2170$ cm^{-1}).[14]

We model all metal surfaces with a five-layer slab with 12 Å vacuum within the three-dimensionally periodic supercell. The bottom two layers are kept fixed in bulk positions to represent the semi-infinite bulk crystal beneath the surface. We find that using two more layers of metal substrate (and relaxing one more layer) only changes the adsorption energy by $\sim$0.03 eV/CO, which is within the error of the calculations. We use five layers of Fe atoms to model Fe(100) and one layer of Al on top of four layers of Fe to model a monolayer of Al on Fe(100) [Al/Fe(100)]. To separate strain and chemical effects on CO surface chemistry, we also examine two relevant Al(100) surfaces for comparison: a hypothetical bcc Al(100), which has Al atoms placed in the equilibrium lattice positions of Fe(100), and the ground-state face-centered-cubic (fcc) phase of Al(100). Spin-polarized calculations are employed for Fe(100) and Al/Fe(100), while non-spin-polarized ones are carried out for bcc and fcc Al(100).

Adsorbates are put on one side of the slab; this produces a dipole due to the charge rearrangement on the surface caused by CO adsorption. The correction to the total energy caused by the dipole along the surface normal is included a posteriori and is found to be $\sim$+0.04 eV per CO. The CO molecule is allowed to relax along with the top three layers of each metal substrate.

When the maximum force acting on each atom of the relaxed layers drops below 0.025 eV/Å, the structural relaxation is stopped.

In this study, we explore a CO coverage of 0.25 monolayer (ML) for all surfaces with a $6 \times 6 \times 1$ k mesh, which converges the adsorption (and total) energy to within 0.03 eV/CO. We also explore CO coverages of 0.11 and 0.50 ML for Al/Fe(100) with $3 \times 3 \times 1$ and $12 \times 12 \times 1$ k meshes, respectively. Moreover, we examine the adsorption of isolated C or O atoms on Al/Fe(100) at 0.25 ML coverage to determine the most stable site and then the coadsorption of C and O atoms on Al/Fe(100) at 0.11 ML (the coverage here is with respect to a single species, not the combined coverage of C and O).

To model gaseous CO, and C and O atoms, we place a molecule or atom in a 10 Å cubic box. Highly symmetrical boxes can sometimes produce wrong orbital occupancies for an isolated atom or molecule. If that happens, we can obtain the correct orbital ordering and energy by switching off symmetry or using a near-cubic box (e.g., $10.1 \times 10.2 \times 10.3$ Å). We perform a non-spin-polarized calculation for CO, but spin-polarized calculations for open-shell C and O, where the valence electron configurations used for C and O atoms are triplet $(2s)^2(2p)^2$ and $(2s)^2(2p)^4$, respectively, approximately the ^3P ground state (spin-polarized DFT "wave functions" are slightly spin-contaminated).

The Climbing Image Nudged Elastic Band (CI-NEB) method[34] is used to locate the minimum energy paths (MEPs) and the transition states for CO diffusion and dissociation on Al/Fe(100). The NEB method is a reliable way to find the MEP when the initial and final states of a process are known. An interpolated chain of configurations (images) between the initial and final positions are connected by springs and relaxed simultaneously to the MEP. Once the MEP is nearly converged with the climbing image scheme, the highest-energy image is allowed to climb uphill to the saddle point. In our work, the number of images used is usually between 6 and 12.

Approximate vibrational frequencies of CO on metal surfaces are estimated by diagonalizing a first-order finite-difference construction of the Hessian matrix with displacements of 0.02 Å (only allowing the C and O atoms to move). The natures of the relaxed adsorbate configurations and the saddle points found by the CI-NEB method are checked by analyzing the CO frequencies.

The site-projected and orbital-resolved density of states (DOS) are done with a convenient projection scheme that uses the radial cutoffs of the PAW potentials instead of Wigner–Seitz spheres.[35] Local magnetic moments are obtained from the difference between up-spin and down-spin local DOS integrated up to the Fermi level.

3. Results and Discussion

3.1. Structural and Magnetic Properties of Clean Surfaces. We benchmark the accuracy of the DFT–PAW–GGA method by calculating properties for Fe(100) and Al(100). We then give predictions of properties for Al/Fe(100). Table 1 displays the interlayer relaxation and local magnetic moments for Fe atoms near the surface. Our slab model for Fe(100) reproduces the experimental trend of the slight contraction between the surface and subsurface layers and the slight expansion between the subsurface and the third layers. As reported earlier,[36] our results also agree with previous theoretical work for relaxation of Fe(100). The prediction of a significant enhancement of the magnetic moment for surface Fe atoms agrees very well with a recent experiment of linear magnetic dichroism of the angular

TABLE 1: Interlayer Spacing between Surface and Subsurface Layers (d_{12}), Change in Interlayer Spacings ($\Delta_{i,j}$), and Magnetic Moment for Surface (M_{Fe}) or Subsurface (M_{sub-Fe}) Fe Atoms for Fe(100), Al/Fe(100), and fcc Al(100)

surface	method	d_{12} (Å)	$\Delta_{1,2}$ (%)[a]	$\Delta_{2,3}$ (%)	$\Delta_{3,4}$ (%)	M_{Fe} (μ_B)[b]	M_{sub-Fe} (μ_B)[c]
Fe(100)	PAW−PBE	1.386	−2.2	4.3		2.95	2.35
	expt[d]	1.363	−5 ± 2	5 ± 2		2.84 ± 0.11	-
Al/Fe(100)	PAW−PBE	1.377	−3.5	−2.1	4.1	1.56	2.47
fcc Al(100)	PAW−PBE	2.081	2.9	0			
	expt[e]	1.98−2.13	−2.5 to +5.0				

[a] $\Delta_{i,i+1}$ is defined as the percentage change of interlayer spacing between layer i and $i + 1$, compared with the bulk spacing d_0. For Al/Fe(100), d_0 from bulk Fe is assumed. Layer 1 is the topmost layer, which is an Al layer for Al/Fe(100). [b] This magnetic moment is for the surface Fe atoms of Fe(100) but for the (immediately) subsurface Fe atoms of Al/Fe(100), since the surface atoms are Al, which have nearly zero (ca. −0.04) magnetic moment. [c] This magnetic moment is for the (immediately) subsurface Fe atoms of Fe(100) and for the Fe atoms in the third layer from the surface of Al/Fe(100). [d] Surface relaxation data are from ref 47 and the magnetic moment is from ref 37. [e] References 41−45.

TABLE 2: PAW−DFT−GGA CO Adsorption Energies ($E_{ad} = E_{CO/metal-slab} − E_{metal-slab} − E_{CO}$), CO Bond Lengths ($r_{C-O}$), CO Tilt Angles ($\alpha$) Relative to the Surface Normal, and CO Vibrational Frequencies (ν_{C-O}) for the On-Top and Tilted-Hollow (TH) Configurations of CO on Fe(100), Al/Fe(100), "bcc" Al(100), and fcc Al(100)[a]

substrate	Θ (ML)	site	E_{ad} (eV)	r_{C-O} (Å)[b]	α (deg)	ν_{C-O} (cm^{-1})[b]
Fe(100)	0.25	on top	−1.48 (−1.17)	1.178	0	1895
		TH	−2.08 (−1.49)	1.321	49.6	1189
		expt	−1.11[c]		45 ± 10, 53 ± 2[d]	1210[e]
Al/Fe(100)	0.11	on top	−0.83 (−0.64)	1.165	0	
		TH	−1.00 (−0.54)	1.476	65.0	
	0.25	on top	−0.80 (−0.61)	1.165	0	1949
		TH	−0.99 (−0.44)	1.472	66.2	883
	0.50	on top	−0.82 (−0.62)	1.163	0	
		TH	−0.59 (−0.06)	1.474	61.1	
bcc Al(100)[f]	0.25	on top	−0.45 (−0.26)	1.164	0	1946
		TH	−0.28 (0.15)	1.459	65.0	883
fcc Al(100)	0.25	on top	−0.25 (−0.06)	1.165	0	1951
		TH	−0.42 (0.05)	1.497	55.6	786

[a] RPBE predictions for E_{ad} are shown in parentheses. [b] For gas-phase CO, the experimental bond length is 1.128 Å and the stretching frequency is 2170 cm^{-1},[14] while DFT−GGA(PBE) yields R_e = 1.14 Å and ν_{C-O} = 2158 cm^{-1}. [c] This value was obtained by analyzing temperature-programmed desorption data[50,56] at ∼0.50 ML, assuming simple first-order desorption kinetics with a frequency factor of 10^{13} s^{-1}; our and other DFT results[48,57] show that the E_{ad} values are about the same at 0.25 and 0.50 ML. We note that the actual prefactor for a TPD experiment can reach 10^{17} s^{-1}, which will yield an E_{ad} of −1.26 eV in this case and bring it closer to the DFT−RPBE value. [d] First datum is from near-edge X-ray absorption fine structure (NEXAFS)[58] and second is from X-ray photoelectron diffraction (XPD).[59] [e] Reference 21. [f] Al atoms are placed in the equilibrium lattice positions of Fe(100).

distribution of Fe 3p photoelectron spectral intensities.[37] Our result for the surface magnetic moment is also in line with previous predictions.[38−40] We predict a slight expansion between the two surface layers of Al(100). Low-energy electron diffraction (LEED),[41] surface-extended X-ray absorption fine structure (SEXAFS),[42] and medium electron energy diffraction investigations[43] indicate that Al(100) is bulk-terminated with no surface relaxation. An older LEED study[44] suggests that the interlayer spacing between the surface and subsurface layers of Al(100) expands by 5%, while an MeV ion scattering study shows that the spacing contracts by < 2.5% (or 0.05 Å).[45] We note that the vertical vibrational amplitude of the Al(100) surface layer is quite large (estimated to be ∼0.15 Å at 300 K[46]). As a result, there is a significant error bar associated with the experimental determination of surface relaxation for Al(100).

We see from Table 1 that placing a monolayer of Al on Fe(100) hardly affects the structural properties of the underlying Fe(100) substrate. The interlayer spacing between the surface Al layer and the subsurface Fe layer is similar to the equilibrium spacing d_{12} of Fe(100). Moreover, the interlayer relaxation among Fe layers beneath Al seems to be unaffected by the Al overlayer, as seen by comparing $\Delta_{2,3}$ and $\Delta_{3,4}$ of Al/Fe(100) to $\Delta_{1,2}$ and $\Delta_{2,3}$ of Fe(100), respectively. The Al−Al nearest-neighbor distance in Al/Fe(100) (2.834 Å) is almost equal to that of fcc Al(100) (2.828 Å), so a monolayer of Al on Fe(100) is under very small lateral strain. However, the Al overlayer does influence one property dramatically: it quenches the local magnetic moment of the surface Fe atoms by nearly 50%.

3.2. CO Adsorption. We first present DFT−GGA results for CO adsorption on Fe(100) as a benchmark. Using HREELS, Moon et al. found a tilted state of CO on the hollow site of Fe(100) with an unusually low CO stretching frequency of 1210 cm^{-1}.[21] Our DFT−GGA calculations confirm that CO prefers the tilted hollow site. We obtain a tilt angle of 49.6° and a stretching frequency of 1189 cm^{-1} (see Table 2), which agree quite well with experiment and previous theoretical studies.[48,49] It should be noted, however, that DFT−GGA(PBE) tends to overestimate the binding energy between CO and metal surfaces and that DFT−GGA(RPBE) corrects some of this overbinding, as shown in Table 2. The significant disagreement (∼0.4 eV) that remains between DFT−GGA(RPBE) and experiment[50] for the adsorption energy of CO points to the need for either further measurements (the only one we found was from 20 years ago) or refinement of the description of electron exchange and correlation, either via new functionals or via, e.g., use of a recently proposed configuration interaction (CI) in DFT embedding theory.[51−55] For our purposes, however, the current results provide a measure of error associated with our DFT binding energies, which can be used to better estimate CO binding energies to Al/Fe(100), where experimental values are unavailable.

Next, we investigate the adsorption of CO on Al/Fe(100). We considered several high-symmetry orientations at the on-top (OT), 2-fold bridge, and 4-fold hollow sites. The lowest energy structure at the 2-fold bridge site is found to be a transition state and is not considered further. The structures at the OT and hollow sites found to be the most stable are shown
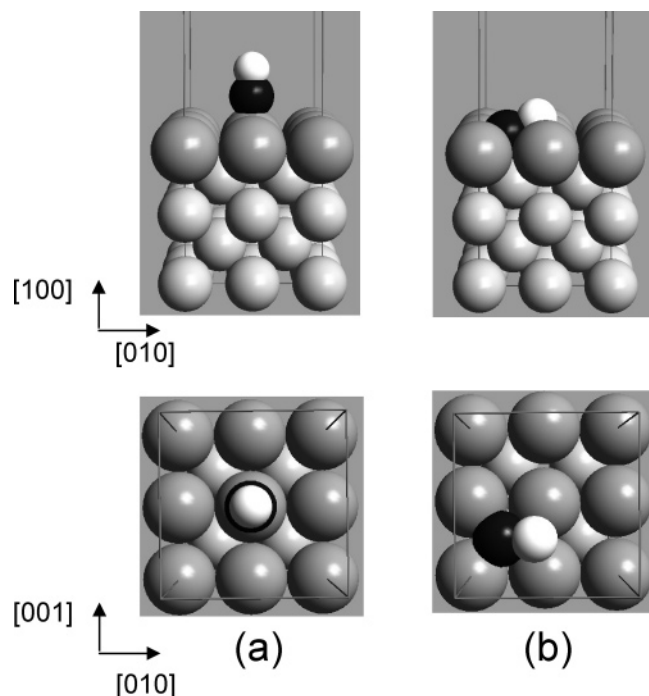
Figure 1. Adsorption structures of CO on Al/Fe(100): (a) on-top; (b) tilted-hollow. Upper panel is the side view, and lower panel, the top view. The color scheme is Al in dark gray, Fe in light gray, C in black, and O in white. The same color scheme is used in all subsequent figures.

Figure 2. Site-projected local densities of states (LDOS) for the sp band of the surface Al atoms of a metal slab before adsorption. The center of gravity of the Al LDOS moves up as the Al layers compress from fcc Al to "bcc" Al(100) and as the subsurface Al atoms are replaced with bcc Fe.

in Figure 1, and Table 2 displays their corresponding predicted properties. At the hollow site, CO is found to be highly tilted. This tilted-hollow (TH) configuration is predicted to have an *extremely low* CO stretching frequency of only 883 cm^{-1} at 0.25 ML, which is only ~40% of the gaseous value! In this most highly tilted configuration, the C atom resides at the 4-fold hollow site, while the O atom is close to the 2-fold bridge site. The C–O bond length in the TH configuration is even larger than that in gaseous methanol ($R(H_3C-OH) = 1.425$ Å[60,61]), indicating that the C–O bond order in this adsite is reduced to ≤1. As mentioned earlier, this TH configuration was previously found experimentally[21,59] and theoretically[48,49,62] for CO/Fe(100). However, CO on Al/Fe(100) is predicted to be tilted even more toward the surface, with a ~300 cm^{-1} lower stretching frequency, and a ~0.15 Å longer bond length than CO on Fe(100) (see Table 2). These unusual predictions for the CO stretching frequency and tilt angle could be verified by such experiments as HREELS[21] and near-edge X-ray absorption fine structure[58] or X-ray photoelectron diffraction,[59] respectively.

Table 2 also shows how the CO adsorption energy changes with coverage (Θ) for the OT and TH sites of Al/Fe(100). We see that E_{ad} varies only slightly (~0.03 eV) with Θ for the OT site. However, the binding of CO to Al/Fe(100) at the TH site is significantly reduced at higher coverage (0.50 ML), indicating that CO in the TH site experiences destabilizing lateral repulsions as the coverage increases. Given its side-on adsorption geometry, it is not surprising that its binding energy is sensitive to coverage. Unfortunately, the relative stability between the OT and TH sites depends not only on coverage (as it should) but also on the choice of GGA functional (which it should not!). GGA–PBE predicts that the OT site is preferred at higher coverage (0.50 ML), with the TH site being more stable at lower coverage (0.11 or 0.25 ML). By contrast, GGA–RPBE predicts that the OT site is preferred for all coverages considered. This qualitative disagreement between two functionals is extremely unsatisfying, again illustrating the lack of definitive
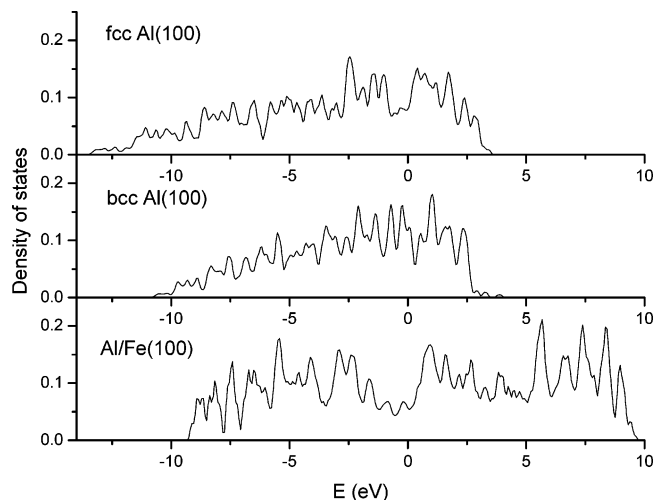
exchange-correlation functionals. Note also that since even RPBE is overbound for CO/Fe(100) by ~0.4 eV, then the TH CO on Al/Fe(100) may be only slightly bound to the surface and only at low coverages.

To deconvolute the interaction between CO and Al/Fe(100), we also examined CO adsorption on two differently constructed Al(100) surfaces. One is an artificial "bcc" Al(100), with Al atoms constrained to reside in the equilibrium lattice positions of Fe(100). The other surface is the natural fcc Al(100) surface, which is unstrained. As mentioned above, the lateral strain within the Al layer is small for both Al/Fe(100) and bcc Al(100). However, "bcc" Al(100) is under significant compressive strain along surface normal because the interlayer distance of "bcc" Al(100) is ~0.6 Å smaller than the natural spacing of 2.0 Å in fcc Al(100).

The CO adsorption data for these two Al surfaces are also displayed in Table 2. The OT and TH states are both minima for CO adsorbed on bcc and fcc Al(100). GGA–PBE predicts that CO is slightly bound at the TH and OT sites on those two surfaces, while GGA–RPBE predicts that CO will not bind to either surface in the TH site and only weakly adsorbs in the OT site. Because RPBE tends to give more reliable adsorption energetics, we believe that CO is not stable on the TH site of bcc or fcc Al(100), indicating that *the Fe substrate is key to stabilizing adsorption of CO on Al/Fe(100)*. Changes in the electronic structure provide supporting evidence for this assertion, as we now discuss.

Table 2 indicates that the adsorption exothermicity of CO on the OT site at 0.25 ML increases going from fcc Al(100) to bcc Al(100) to Al/Fe(100). Because the adsorption structure (for example, the CO bond length and vibrational frequency) at this site is almost the same for those three surfaces, the adsorption energy differences must depend primarily on the electronic properties of the surface Al layer. The site-projected local densities of states of the surface Al sp band for those three clean surfaces are displayed in Figure 2. We see that the center of gravity of the Al sp band moves up in energy, following the same sequence as the CO adsorption exothermicity: fcc Al(100) < bcc Al(100) < Al/Fe(100). This shift in energy leads to more empty states in the Al sp band of Al/Fe(100), resulting in stronger CO–metal interactions via electron donation from the CO 5σ orbital to the empty Al states for CO adsorbed in the
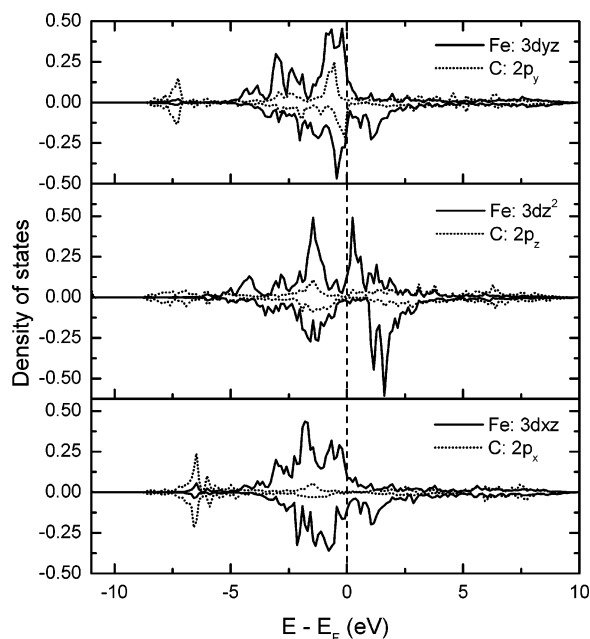
CO on a Monolayer of Al Covering Fe(100)

J. Phys. Chem. B, Vol. 110, No. 44, 2006 **22217**

Figure 3. Spin-polarized, site-projected, orbital-resolved LDOS for the carbon atom and the surface Fe atom under C of CO/Al/Fe(100) at the tilted-hollow site. The z direction is along the surface normal, with x along [010]; see Figure 1. Up (majority) spin LDOS given as positive, down (minority) spin LDOS as negative.

OT site. This argument is in the same spirit employed by Hammer and Nørskov to correlate the d-band centers of transition metal surfaces to their chemical properties.[63] In their analysis, the contribution from the sp band is assumed not to change from metal to metal (or in alloys). This is valid for transition metals because the surface chemical bonding there is dominated by d electrons and the sp band is rather dispersed. In our case, the surface Al layer provides only sp electrons to interact with CO, so we expect here we have to explicitly consider the role of the sp band.

Now we consider what makes CO more stable at the TH site of Al/Fe(100) compared to the analogous sites on "bcc" and fcc Al(100). In fcc Al(100), the subsurface Al layer is quite far away from the surface layer (~2.0 Å). Direct interaction of CO with the subsurface Al atom should be negligible here. The highly tilted state of CO at the TH site is found to be weakly attractive by GGA−PBE (and slightly repulsive by GGA−RPBE) on this surface. When we bring the subsurface Al layer closer to the surface Al layer in "bcc" Al(100), the interaction between CO and the surface becomes less attractive by GGA−PBE (and even more repulsive by GGA−RPBE). However, if we replace the subsurface Al layers with Fe in Al/Fe(100), the interaction between CO and the surface becomes more attractive. As mentioned above, this seems to indicate an interaction of CO with the subsurface Fe atoms of Al/Fe(100). To pinpoint this interaction, we display in Figure 3 the orbital-resolved LDOS for the C atom of CO and the subsurface Fe atom below C. We see that strong orbital mixing occurs between C $2p_y$ and Fe $3d_{yz}$ due to the near degeneracies between those states. This suggests a significant interaction of C with the subsurface Fe atom, involving an unorthodox π-type bonding interaction (since the C $2p_y$ is roughly parallel to the surface). Relatively weaker orbital mixing takes place between C $2p_z$ and Fe $3d_{z^2}$, as well as between C $2p_x$ and Fe $3d_{xz}$. Thus, the stabilization of CO on Al/Fe(100) involves a π-type bonding interaction between C and a subsurface Fe atom. This is further supported by a plot of the electron density change upon adsorption (Figure 4). We see that dramatic rearrangements of electron density occur, with
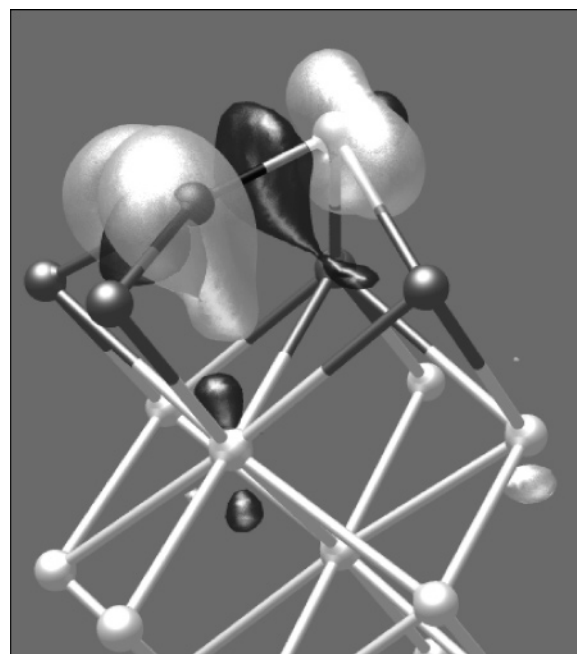

Figure 4. Isosurface plot of the electron density difference, $\Delta\rho$, for CO/Al/Fe(100) at the tilted-hollow site. The isosurface value is at 0.075 e/Å³ for the light gray surface and −0.075 e/Å³ for the dark gray surface. Negative $\Delta\rho$ indicates loss of electron density upon adhesion. Solid balls represent atoms.

π_y-type symmetry evident for the charge accumulation in the light gray isosurface. Electron density is depleted from three major areas along the C−O bond axis (C terminal, C−O σ bond, and O terminal regions) and polarizes toward the surface Al atoms and the subsurface Fe atom.

3.3. CO Diffusion and Dissociation on Al/Fe(100). We first examine CO diffusion from the OT site to the TH site on Al/Fe(100). The MEP is shown in Figure 5, for $\Theta_{CO} = 0.11$ ML. We see that the PBE (RPBE) functional gives a fairly high diffusion barrier of 0.64 (0.84) eV. We find that CO can also diffuse from one OT site to another via a 2-fold bridge site with a much lower barrier (~0.25 eV for both PBE and RPBE, not shown in Figure 5). Thus, CO diffusion between OT sites should occur readily, whereas diffusion to the TH site is predicted to be a much rarer event.

CO dissociation on metal surfaces is often thought to begin with a tilted adsorption state characterized by an elongated CO bond and decreased CO stretching frequency, as on Fe(100). Even on surfaces where the OT site is preferred, such as on Fe(110), CO dissociation has been predicted to proceed first via CO diffusing off the OT site to a high coordination site and then tilting its molecular axis almost parallel to the surface to dissociate at a bridge site.[64] On Al/Fe(100), it is natural to envision CO dissociating at the TH site in the same manner as on Fe(100). Before characterizing the reaction pathway, however, it is necessary to learn where C and O atoms prefer to adsorb on Al/Fe(100) after CO dissociation, to establish the final state of the MEP. We find that C prefers the 4-fold hollow site on Al/Fe(100), with this hollow site being the only energy minimum (Table 3). Both the bridge site and the hollow site are local minima for O, with the bridge site ~0.3 eV more stable. Figure 5 depicts the energy profile of CO dissociation from the TH site, leading to C at the hollow site and O at the bridge site on Al/Fe(100). The dissociation has a barrier of 0.38 eV (GGA−PBE), which is ~0.70 eV smaller than the analogous CO dissociation process on Fe(100),[48] while GGA−RPBE yields an even smaller barrier (0.33 eV).
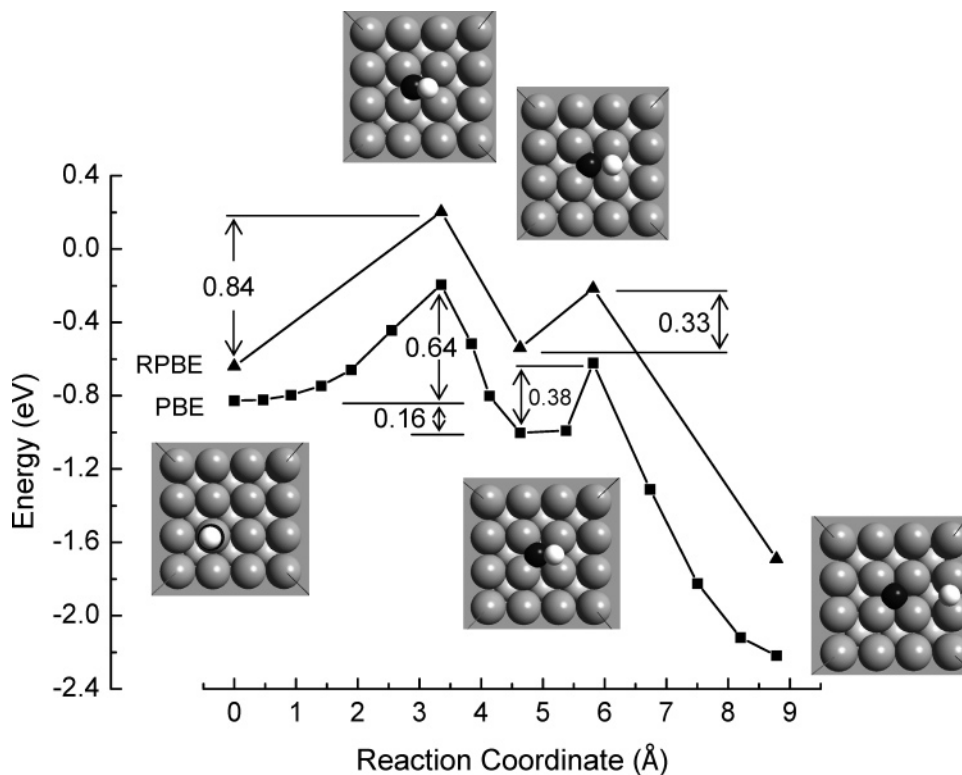
Figure 5. PAW−DFT−GGA−PBE minimum energy path for CO diffusion from the on-top site to the tilted-hollow site and subsequent dissociation at the tilted-hollow site at $\theta_{CO} = 0.11$ ML. The RPBE energies are shown for the critical points only. The energy of a pure metal slab plus an isolated gaseous CO molecule is set as zero.

TABLE 3: Adsorption Energies ($E_{ad} = E_{x=C,O/Fe-slab} - E_{Fe-slab} - E_{x=C,O}$) for Isolated C or O atoms on Al/Fe(100) at 0.25 ML by PAW−DFT−GGA−PBE[a]

species	on-top	bridge	hollow
$E_{ad,C}$ (eV)	−2.94 (hos)	−5.08 (ts)	−7.00 (min)
$E_{ad,O}$ (eV)	−4.91 (hos)	−6.71 (min)	−6.42 (min)

[a] The nature of the critical point is given in parentheses (min = minimum, ts = transition state, and hos = higher order saddle point).

If we consider CO diffusion and CO dissociation simultaneously, we observe that the PBE and RPBE functionals suggest qualitatively different scenarios. The PBE functional predicts that the TH adsorption site is preferred, with only a small barrier (0.38 eV) to dissociation from this site. Heating up CO adsorbed at the TH site will cause CO dissociation instead of desorption ($E_{des} = 1.00$ eV) or diffusion to the OT site ($E_{diff} = 0.80$ eV), while heating CO adsorbed at the OT site will cause CO diffusion from the OT site to another OT site ($E_a = 0.24$ eV) or to the TH site ($E_a = 0.64$ eV) instead of desorption ($E_a = 0.83$ eV). Either way, once at the TH site, CO will readily dissociate. By contrast, the RPBE functional predicts that while the TH adsite is stable, the OT site is preferred. Moreover, because the barrier for CO diffusion between the OT and TH sites is greater than the desorption energy for CO at either the OT site or the TH site (see Figure 5), these two sites are predicted by DFT−RPBE to not be directly interconvertible. Therefore, the RPBE functional predicts that CO may only be trapped at the TH site at lower temperatures; subsequent heating of CO adsorbed at this site will cause CO dissociation. On the other hand, DFT−RPBE predicts that heating CO at the OT site will cause CO diffusion to another OT site and ultimately desorption rather than dissociation. The discrepancies between the qualitative conclusions from the two exchange-correlation functionals, namely, that only some CO will dissociate (according to RPBE) rather than all adsorbed CO (according to

PBE), points again to the problems with current exchange-correlation functionals for DFT. Nevertheless, it is clear that either functional does suggest from the lowered barriers an enhanced CO dissociation rate on Al/Fe(100) compared to pure Fe(100).

4. Summary

We used periodic slab density functional theory (DFT) to characterize CO adsorption, diffusion, and dissociation energetics on the Al/Fe(100) surface, which consists of one monolayer of Al adsorbed on the (100) surface of ferromagnetic bcc Fe. We used the DFT−GGA−PBE functional for all geometry relaxations and also applied the DFT−GGA−RPBE functional to the PBE-optimized structures to correct the adsorption energetics, since RPBE has been shown to generally provide better adsorption energetics.[30] We find that the Al monolayer greatly reduces the surface magnetic moment of Fe(100) but changes its structural relaxation only slightly. A weakly chemisorbed state of CO on Al/Fe(100) is predicted to form with unusual properties more conventionally found for strongly chemisorbed molecules. We find that CO can adsorb on the 4-fold hollow site in a highly tilted fashion, with a bond length reminiscent of a C−O single bond and an extremely low CO stretching frequency of only 883 cm^{-1}, *lower than any previously reported CO stretching frequency on a metal surface*. All of these metrics indicate a dramatically weakened CO bond relative to gaseous CO (stretching frequency at 2170 cm^{-1}). Another adsorption site is found to be the upright adsorption of CO on the on-top site of Al/Fe(100). DFT−GGA−PBE predicts that the TH site is preferred at coverages below 0.5 ML, while DFT−GGA−RPBE predicts that the OT site is preferred for all coverages studied (0.11−0.5 ML). This discrepancy indicates the need for better exchange-correlation functionals for DFT.

We compared CO adsorption on Al/Fe(100) with adsorption on fcc Al(100) and a hypothetical strained bcc Al(100) (with Al replacing Fe in the equilibrium structure of Fe(100)). Although the tilted hollow state of CO is also predicted to be weakly bound on bcc and fcc Al(100) by DFT−GGA−PBE, DFT−GGA−RPBE does not predict this tilted state to be stable. Analysis of the local density of states of CO/Al/Fe(100) shows that the tilted state of CO is stabilized by a π-type orbital mixing between the C atom and the subsurface Fe atom under C. CO is found to be weakly bound on the on-top site in a upright fashion on bcc and fcc Al(100). CO binds more strongly at the on-top site of Al/Fe(100) than on bcc or fcc Al(100), because the Al sp band of Al/Fe(100) is affected by the underlying Fe layers and moves up in energy, thereby emptying more states so as to better bind with CO via CO 5σ lone pair donation into empty metal states.

We obtained the minimum energy paths for CO diffusion and dissociation on Al/Fe(100) at 0.11 ML coverage. Once again, the two exchange-correlation functionals lead to somewhat different predictions. DFT−GGA−PBE predicts that all CO molecules ultimately end up at the TH site and then dissociate. DFT−GGA−RPBE predicts that only those CO molecules trapped at the TH site will dissociate; heating CO adsorbed at the OT site will lead to CO diffusion among the OT sites and ultimately desorption, instead of dissociation or diffusion to the TH site, followed by dissociation. Nevertheless, both functionals predict that CO adsorbed at the TH site dissociates more readily ($E_a = 0.33-0.38$ eV) than diffuses or desorbs. This low barrier to dissociation, compared to 1.10 eV on Fe(100), suggests that an Fe-supported Al monolayer can activate CO more easily. This information may be useful for designing low-temperature CO hydrogenation catalysts.

References and Notes

(1) Sinfelt, J. H. *Sci. Am.* **1985**, *253*, 90.
(2) Sinfelt, J. H. *Acc. Chem. Res.* **1987**, *20*, 134.
(3) Campbell, C. T. *Annu. Rev. Phys. Chem.* **1990**, *41*, 775.
(4) Campbell, C. T.; Goodman, D. W. *J. Phys. Chem.* **1988**, *92*, 2569.
(5) Pelzer, T.; Grune, M.; Wandelt, K. *Prog. Surf. Sci.* **2003**, *74*, 57.
(6) Chen, J. G.; Crowell, J. E.; Ng, L.; Basu, P.; Yates, J. T. *J. Phys. Chem.* **1988**, *92*, 2574.
(7) Koel, B. E.; Smith, R. J.; Berlowitz, P. J. *Surf. Sci.* **1990**, *231*, 325.
(8) Heitzinger, J. M.; Geghard, S. C.; Koel, B. E. *Surf. Sci.* **1992**, *275*, 209.
(9) Hwu, H. H.; Eng, J.; Chen, J. G. *J. Am. Chem. Soc.* **2002**, *124*, 702.
(10) Khan, N. A.; Hwu, H. H.; Chen, J. G. *J. Catal.* **2002**, *205*, 259.
(11) Kitchin, J. R.; Khan, N. A.; Barteau, M. A.; Chen, J. G.; Yakshinksiy, B.; Madey, T. E. *Surf. Sci.* **2003**, *544*, 295.
(12) Kitchin, J. R.; Nørskov, J. K.; Barteau, M. A.; Chen, J. G. *Phys. Rev. Lett.* **2004**, *93*.
(13) Anderson, R. B. *The Fischer−Tropsch Synthesis*; Academic Press: Orlando, FL, 1984.
(14) Huber, K. P.; Herzberg, G. *Molecular Spectra and Molecular Structure, 4: Constants of Diatomic Molecules*; Van Norstrand Reinhold Co.: New York, 1979.
(15) Blyholder, G. *J. Phys. Chem.* **1964**, *68*, 2772.
(16) Sung, S. S.; Hoffmann, R. *J. Am. Chem. Soc.* **1985**, *107*, 578.
(17) Greeley, J.; Nørskov, J. K.; Mavrikakis, M. *Annu. Rev. Phys. Chem.* **2002**, *53*, 319.
(18) Pavão, C.; Guimarães, T. C. F.; Lie, S. K.; Taft, C. A.; Lester, W. A., Jr. *Theochem* **1999**, *458*, 99.
(19) Paul, J. *Nature (London)* **1986**, *323*, 701.
(20) Paul, J.; Hoffmann, F. M. *J. Chem. Phys.* **1987**, *86*, 5188.
(21) Moon, D. W.; Bernasek, S. L.; Dwyer, D. J.; Gland, J. L. *J. Am. Chem. Soc.* **1985**, *107*, 4363.
(22) Paul, J.; Hoffmann, F. M. *Chem. Phys. Lett.* **1986**, *130*, 160.
(23) Hohenberg, P.; Kohn, W. *Phys. Rev.* **1964**, *136*, B864.
(24) Kohn, W.; Sham, L. J. *Phys. Rev.* **1965**, *140*, A1133.
(25) Kresse, G.; Furthmüller, J. *Phys. Rev. B* **1996**, *54*, 11169.
(26) Kresse, G.; Furthmüller, J. *Comput. Mater. Sci.* **1996**, *6*, 15.
(27) Blöchl, P. E. *Phys. Rev. B* **1994**, *50*, 17953.
(28) Kresse, G.; Joubert, D. *Phys. Rev. B* **1999**, *59*, 1758.
(29) Perdew, J. P.; Burke, K.; Ernzerhof, M. *Phys. Rev. Lett.* **1998**, *80*, 891.
(30) Hammer, B.; Hansen, L. B.; Nørskov, J. K. *Phys. Rev. B* **1999**, *59*, 7413.
(31) Monkhorst, H. J.; Pack, J. D. *Phys. Rev. B* **1976**, *13*, 5188.
(32) Methfessel, M.; Paxton, A. T. *Phys. Rev. B* **1989**, *40*, 3616.
(33) Jiang, D. E.; Carter, E. A. *Phys. Rev. B* **2003**, *67*, 214103.
(34) Henkelman, G.; Uberuaga, B. P.; Jónsson, H. *J. Chem. Phys.* **2000**, *113*, 9901.
(35) Kresse, G.; Furthmüller, J. VASP the Guide. Available from http://cms.mip.univie.ac.at/VASP/.
(36) Jiang, D. E.; Carter, E. A. *J. Phys. Chem. B* **2004**, *108*, 19140.
(37) Panaccione, G.; Sirotti, F.; Rossi, G. *Solid State Commun.* **2000**, *113*, 373.
(38) Wang, C. S.; Freeman, A. J. *Phys. Rev. B* **1981**, *24*, 4364.
(39) Fu, C. L.; Freeman, A. J.; Oguchi, T. *Phys. Rev. Lett.* **1985**, *54*, 2700.
(40) Eriksson, O.; Fernando, G. W.; Albers, R. C.; Boring, A. M. *Solid State Commun.* **1991**, *78*, 801.
(41) Aberdam, D.; Baudoing, R.; Gaubert, C.; McRae, E. G. *Surf. Sci.* **1976**, *57*, 715.
(42) Bianconi, A.; Bachrach, R. Z. *Phys. Rev. Lett.* **1979**, *42*, 104.
(43) Masud, N.; Baudoing, R.; Aberdam, D.; Gaubert, C. *Surf. Sci.* **1983**, *133*, 580.
(44) Marcus, P. M.; Jepsen, D. W.; Jena, P. *Surf. Sci.* **1972**, *31*, 180.
(45) Cheng, H. S.; Chui, Z. X.; Xu, H. J.; Yao, X. W.; Yang, F. J. *Nucl. Instrum. Methods Phys. Res., Sect. B* **1990**, *45*, 424.
(46) Zivieri, R.; Santoro, G.; Bortolani, V. *Phys. Rev. B* **1999**, *59*, 15959.
(47) Wang, Z. Q.; Li, Y. S.; Jona, F.; Marcus, P. M. *Solid State Commun.* **1987**, *61*, 623.
(48) Sorescu, D. C.; Thompson, D. L.; Hurley, M. M.; Chabalowski, C. F. *Phys. Rev. B* **2002**, *66*, 035416.
(49) Nayak, S. K.; Nooijen, M.; Bernasek, S. L.; Blaha, P. *J. Phys. Chem. B* **2001**, *105*, 164.
(50) Moon, D. W.; Dwyer, D. J.; Bernasek, S. L. *Surf. Sci.* **1985**, *163*, 215.
(51) Govind, N.; Wang, Y. A.; da Silva, A. J. R.; Carter, E. A. *Chem. Phys. Lett.* **1998**, *295*, 129.
(52) Govind, N.; Wang, Y. A.; Carter, E. A. *J. Chem. Phys.* **1999**, *110*, 7677.
(53) Klüner, T.; Govind, N.; Wang, Y. A.; Carter, E. A. *Phys. Rev. Lett.* **2001**, *86*, 5954.
(54) Klüner, T.; Govind, N.; Wang, Y. A.; Carter, E. A. *Phys. Rev. Lett.* **2002**, *88*, 209702.
(55) Klüner, T.; Govind, N.; Wang, Y. A.; Carter, E. A. *J. Chem. Phys.* **2002**, *116*, 42.
(56) Cameron, S. D.; Dwyer, D. J. *Langmuir* **1988**, *4*, 282.
(57) Bromfield, T. C.; Ferre, D. C.; Niemantsverdriet, J. W. *ChemPhysChem* **2005**, *6*, 254.
(58) Moon, D. W.; Cameron, S.; Zaera, F.; Eberhardt, W.; Carr, R.; Bernasek, S. L.; Gland, J. L.; Dwyer, D. J. *Surf. Sci.* **1987**, *180*, L123.
(59) Saiki, R. S.; Herman, G. S.; Yamada, M.; Osterwalder, J.; Fadley, C. S. *Phys. Rev. Lett.* **1989**, *63*, 283.
(60) Lide, D. R. *Handbook of Chemistry and Physics*, 77th ed.; CRC Press: Boca Raton, FL, 1996.
(61) The R(H$_3$C−OH) from our DFT−GGA calculation is 1.430 Å.
(62) Blyholder, G.; Lawless, M. *J. Chem. Soc., Chem. Commun.* **1990**, 632.
(63) Hammer, B.; Nørskov, J. K. *Adv. Catal.* **2000**, *45*, 71.
(64) Jiang, D. E.; Carter, E. A. *Surf. Sci.* **2004**, *570*, 167.